The Microstructural Characterization, Physical and Dynamic Magnetic Properties of $(Ni_{49}Fe_{51})_{100-x}Cr_x$ (x = 0,3,7) Thin Sheets

SOBHAN MOHAMMADI FATHABAD, FARZAD SHAHRI, and REZA GHOLAMIPOUR

In this work, the effects of Cr on the microstructure, physical, and AC magnetic properties of the $Ni_{49}Fe_{51}$ alloy was studied. In this respect, three series of thin sheets of $(Ni_{49}Fe_{51})_{100-x}Cr_x$ (x = 0, 3, and 7 at. pct) alloys with a final thickness of 120 μm were prepared by means of severe cold rolling and an 1150 °C annealing process at H_2 atmosphere. Optical microscopy (OM), scanning electron microscopy (SEM), X-ray diffraction (XRD), (200) X-ray pole figure, and magnetic force microscopy (MFM) were employed to study microstructure, texture, and magnetic domain structure of the alloys. The magnetic characteristics of the samples were evaluated using BH-hysteresis loop tracer at a frequency range of 0.5 to 300 Hz. Based on the results obtained, it was shown that the mean magnetic domain width was increased from 1.006 to 1.398 μm for 0 Cr and 7 Cr samples, respectively. Furthermore, the magnitude of the static hysteresis loss increased and the excess and classical eddy current loss decreased for the Cr-added thin sheets.

I. INTRODUCTION

50NI-FE alloys have a high saturation induction (about 1.5 T) and a great relative permeability (10 to 55 thousands).[1] These remarkable soft magnetic properties have attracted them wide interest for a variety of applications such as transformer cores, relays, low power consumption signal transformations, electronic sensors, magnetic seal systems, and moderate frequency electromagnetic field shielding.[2,3]

Theses alloys are produced in sheet form by five basic processes: (I) ingot casting, (II) homogenizing of the ingot, (III) hot rolling, (IV) cold rolling, and finally, (V) reducing atmosphere annealing in hydrogen.[4–10] It has already shown that most of the soft magnetic materials are used in the forms of sheets or tapes and therefore, cold rolling is an important process in the production of theses alloys.[11] For the $Ni_{50}Fe_{50}$ alloys, stacking fault energy (SFE) is about 100 mJ m^2,[12] which makes them easy to cold roll down to a micro-scale thickness.[12] The improvement of soft magnetic properties mainly relies on the additives and development of final texture and phases through the cold rolling process and suitable heat treatment.[14–17] It is shown that based on the cold rolling degree, a random oriented or a cube texture can be formed during the subsequent annealing.[13,14] Cube-textured $Ni_{50}Fe_{50}$ alloys are well known for application such as tape toroidal magnetic amplifier cores and radar pulse transformers.[1]

Among the various additives studied, the substitution of Cr for Fe and Ni atoms has been reported to increase the hardness and resistivity and to decrease saturation magnetization and coercivity of the $Ni_{50}Fe_{50}$ alloys.[6,7,15] However, the effect of Cr was not investigated on the dynamic magnetic properties of these alloys. Various works have investigated the dynamic magnetic properties of soft magnetic materials by determining the core loss using AC hysteresis loop tracer, *e.g.*, References 16 through 18. The Core loss, as an extrinsic magnetic property, mainly relies on the composition and development of appropriate microstructure and texture through production process conditions. It is shown that the total core loss per magnetization cycle (J m^{-3}) of a magnetic core consists of three contributing sources related to the static

SOBHAN MOHAMMADI FATHABAD is with Department of Engineering and High-Tech., Iran University of Industries and Mines, Tehran, Iran. FARZAD SHAHRI and REZA GHOLAMIPOUR are with the Department of Advanced Materials and Renewable Energy, Iranian Research Organization for Science and Technology, Tehran, Iran. Contact e-mail: Fshahri@irost.ir

hysteresis loss,[2,11] W_{hyst}, classical eddy current loss, W_{cls}, and the excess eddy current loss, W_{exc}. The core loss is shown to be expressed by Ref. [19]

$$W = W_{\mathrm{hyst}} + W_{\mathrm{cls}} + W_{\mathrm{exc}}$$
$$= 4k_{\mathrm{hyst}}B_{\mathrm{max}}^{\alpha} + \frac{\pi^2 t^2}{6\rho} B_{\mathrm{max}}^2 f + \frac{k_{\mathrm{exc}}}{\sqrt{\rho}} B_{\mathrm{max}}^{3/2} f^{1/2} \quad [1]$$

where f is the frequency and B_{max} is the amplitude of sinusoidal magnetic induction, ρ is resistivity and t is the thickness of the sample. It is shown that the hysteresis loss is affected by the defect structures interacting with the material's magnetic domain walls and magnetization process.[20] The α and k_{hyst} in the Eq. [1] represent the effect of defects on the core loss. The k_{exc} represents the effect of microstructure such as grain size fluctuations or wavelengths of stresses.[2]

Based on the model developed by Maxwell's electromagnetism equation for sinusoidal flux density, it is shown that the classical eddy current loss throughout the thickness of an isotropic sample, considering constant permeability and no skin effect, can be expressed by Reference 21

$$W_{\mathrm{cls}} = \frac{\pi^2 t^2}{6\rho} B_{\mathrm{max}}^2 f \quad [2]$$

The excess eddy current loss is attributed to the non-sinusoidal, non-uniform, and non-repetitive domain wall motion.[22] Various models have been developed for describing the excess loss.[23–26] Bertotti et al.[27] from a statistical point of view, showed that the excess core loss of crystalline materials decreases by increasing the active domain walls ($\bar{n}$) by considering that

$$W_{\mathrm{exc}} = \frac{8\sqrt{GSV_0}}{\sqrt{\rho}} B_m^{3/2} f^{1/2} - \frac{\bar{n}_0 V_0}{4f}, \quad [3]$$

where S is the cross-section area of the sample, G is a dimensionless damping parameter, and $\bar{n}_0$ is simultaneously active domain walls when $f \approx 0$ and a magnetic field of V_0. When considering a sample with fine domain structure, the $\bar{n}_0 V_0 / 4f$ term can be neglected due to the activation of domain walls in dynamic condition and the deletion of any memory of the quasi-static state. Improvement of dynamic magnetic properties of the alloys containing fine domain structures has also been reported by Overshott[28] and Li et al.[18] in nanocrystalline materials.

Considering the relationship between magnetic domain structure and core loss mechanisms, it can be concluded that the materials with fine domain structures, i.e., when the number of domain walls is enormously large (i.e., domain width/sheet thickness < 0.2), the velocity of an individual wall is expected to be small. Thus, the magnetization process should be quite homogeneous and consequently, the classical eddy current loss should dominate the total core loss.[11,25,29] The work presented here was therefore inspired by considering possible advantages of the addition of Cr on microstructure and magnetic core loss of $(Ni_{49}Fe_{51})Cr$ thin sheets.

II. MATERIALS AND EXPERIMENTAL METHODS

Ni-Fe alloys ingots, of nominal compositions $(Ni_{49}Fe_{51})_{100-x}Cr_x$ ($x = 0$, 3, 7), were prepared using extra-pure constituting elements by Vacuum Arc Remelting (VAR, FZKH-300VAR-I furnace) in ultra-high-purity Ti-gettered Ar atmosphere on a water-cooled copper crucible. Each alloy was remelted three times to ensure compositional homogeneity and finally, the prepared melt was poured into a $3 \times 2 \times 4$ cm copper mold.

The prepared ingots were homogenized at 1150 °C for 3 hours and then hot rolled at 1100 °C to 800 °C with a 50 pct thickness reduction. In order to investigate the effect of Cr on the microstructure and magnetic properties, only the samples with similar microstructures were chosen for the subsequent cold rolling process. The average grain size of the 0 Cr, 3 Cr, and 7 Cr samples after the hot rolling process was about 99, 96, and 98 ± 2 μm, respectively. The billets were cold rolled with 99 pct thickness reduction (final thickness of 120 μm). The prepared sheets were annealed at 1150 °C for 3 hours in a dry H_2 atmosphere, and then the samples were cooled inside the furnace to 200 °C, followed by an air-cooling to room temperature.

The microstructural study of the thin sheets was carried out using an optical microscope (Olympus BX60) and a field emission scanning electron microscope (Mira II LMU Tescan FE-SEM) at an accelerating voltage of 20 kV equipped with an energy-dispersive X-ray spectrometer (EDS). The metallographic samples were electro-etched using 30 mL methanol and 10 mL HNO_3 electrolyte etchant. The grain size of the samples was measured on three planes (i.e., RDTD, RDND, and TDND planes), and the average size of them was determined using the standard linear-intercept method.[30] Here, the RD, TD, and ND demonstrate the rolling, transverse, and normal directions in the thin sheets, respectively.

The crystalline structure of the annealed samples was examined by X-ray diffraction technique using PHILIPS-PW1730 and Cu-$K_{\alpha 1}$ radiation. The lattice parameters were determined using Nelson–Riley extrapolation method[31] with error estimation about ± 0.002 Å. X-ray pole figures were surveyed on (200) fcc planes in 5 deg steps using Co-$K_{\alpha 1}$ radiation. Vickers microhardness measurements were carried out on the polished RDND surface of thin sheets using Reicher-Duromat 4000E instrument. Five indentations were averaged for each sample.

The room temperature electrical resistivity of the samples was measured with a square four-point probe technique using PROVA-700 instrument. Considering an infinite 2D sheet, the specific electrical resistivity values were determined by Reference 32

$$\rho_{2D}^2 = 2\frac{\pi t}{\ln 2}\frac{V}{I}F, \quad [4]$$

where t is the thickness of the sheet and F is the correction factor.

The magnetic microstructure of the samples was investigated using Magnetic Force Microscopy (MFM, ARA-AFM Advanced Multi-mode). In order to obtain equilibrium domain patterns, samples were demagnetized at 10 Hz, then their surface was scanned using Co-Cr tip. The obtained MFM images of the samples show stray fields of magnetic domain walls, therefore a derivative was performed on them in order to distinguish magnetic domains and domain wall in the images. The procedure will be discussed later in details in another paper. Domain widths were estimated using average intersection distance of domain walls with random test lines within three MFM images for each specimen.

The dynamic B-H loop and magnetic core loss $(J m^{-3})$ at a frequency range of 0.5 to 300 Hz were determined on the ring-shape samples which were prepared according to ASTM A34 standard[33] using a B-H loop tracer.

III. RESULTS AND DISCUSSION

A. *Microstructure and Physical Properties*

Figure 1a shows the microstructure of 7 Cr-annealed sample. It can be seen that primary recrystallized grains are uniformly distributed in the microstructure. The grain size distribution of the annealed alloys is also shown in Figure 1(b). Various reports have confirmed the bimodal distribution of grain size during secondary recrystallization process.[34] It is well known that the rate of nucleation increases with increasing degree of cold work in heavily deformed materials.[35–37] Therefore, in the annealing process, more nuclei are produced due to the severe cold rolling with 99 pct area reduction and accordingly a fine-grained structure is created in the specimens.

Figure 2 shows XRD multiplot patterns of annealed 0 Cr, 3 Cr, and 7 Cr samples. As can be realized in this figure, only one high intensity peak (around $2\theta \approx 51°$ XRD patterns of the samples. The identified peak could be indexed as (200) austenite γ(FeNi) phase with fcc structure.[38] Here the comparison of XRD patterns obtained for these three alloys shows that by increasing of Cr up to 7 at. pct, the intensity of observed diffraction (200) peak increases. This could be suggesting the formation of stronger texture in the Cr-added alloys.[39]
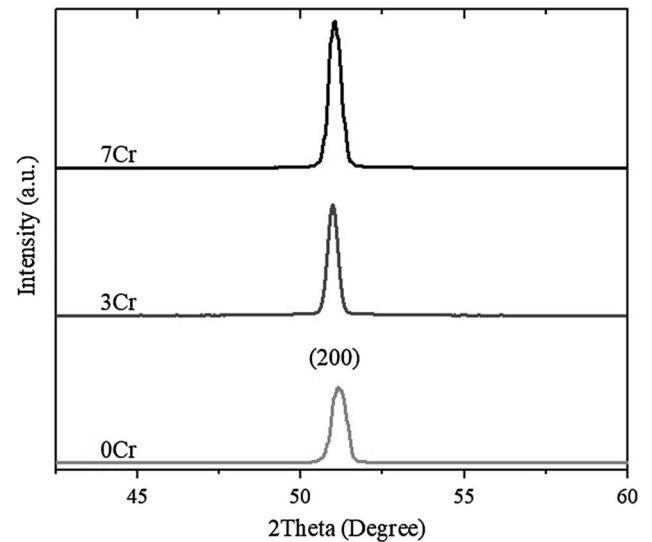

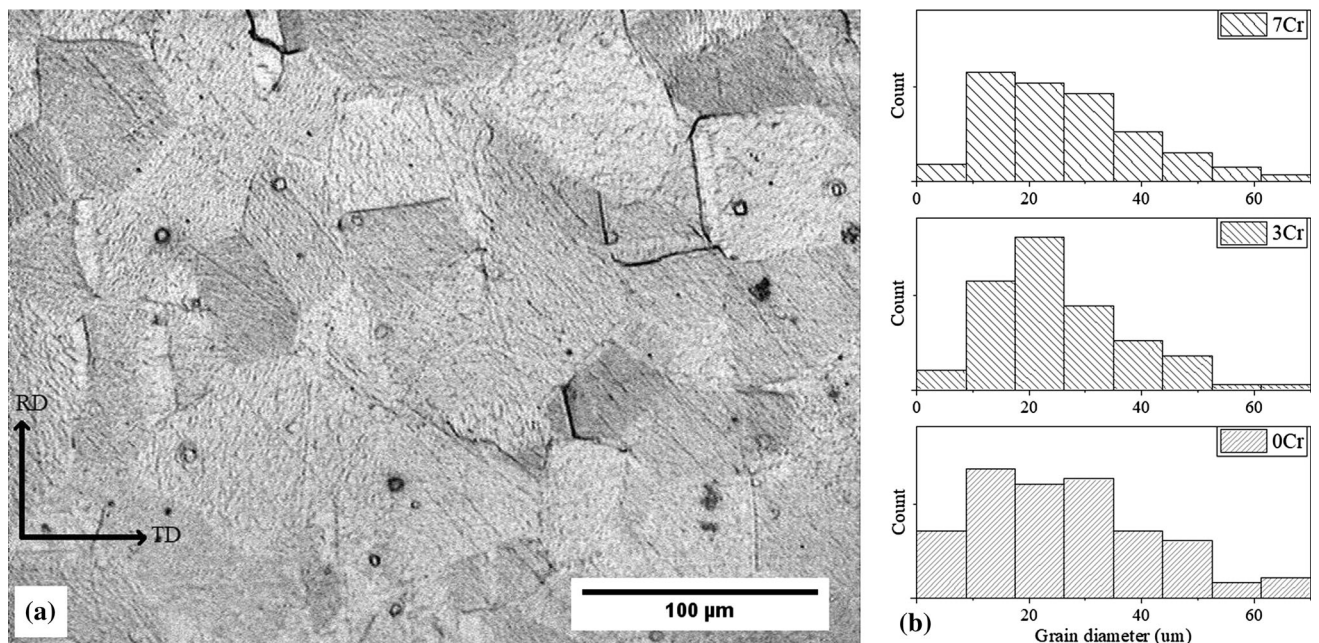Fig. 2—X-ray diffraction patterns of $(Ni_{49}Fe_{51})$ Cr thin sheets for the annealed samples.

Fig. 1—(*a*) Optical microscope image of annealed 7 Cr, (*b*) grain size distribution of 0 Cr, 3 Cr, and 7 Cr.

Pole figure results of annealed 0 Cr and 3 Cr samples are presented in Figures 3(a) and (b). Here, the observed sharp [001] orientation in the pole figures highlights the formation of cube texture in the samples. Previous studies[40,41] have reported that if a highly sharp cube orientation can be formed during the primary recrystallization process, then the strength of cube components improves during the high-temperature annealing process due to the lack of secondary "nuclei" among the primary recrystallized grains. In this work, a high degree of cold rolling has provided enough stored energy for the formation of cube texture.

Table I summarizes various refined parameters obtained for the as-rolled and annealed samples. The microstructural observations revealed that the average grain size of the samples is slightly decreased by adding Cr in the $(Ni_{49}Fe_{51})_{100-x}Cr_x$ alloys. This is due to the lower diffusion rate of grain boundaries in the Cr-added alloys during the recrystallization process.[42]

On the other hand, as it is shown in Table I, the mean microhardness is increased for the Cr-added as-rolled samples. Čebron et al.[43] have reported a directly proportional relationship between hardness and stored energy during the cold rolling process. Here, the observed rising of microhardness with increasing of Cr is in close agreement with the rising of lattice parameter in the Cr-added as-rolled samples. The smaller microhardness for the annealed 7 Cr sample (i.e., 137 Hv for 7 Cr in comparison to 142 Hv for 0 Cr) indicates a higher

degree of recovery transformation during annealing process for the Cr-added samples.[44,45]

The calculated lattice parameters of the annealed 0 Cr sample, based on XRD results, was 3.5707 Å, which is in close agreement with previous reports.[46] The γ(Fe, Ni) phase of the $Ni_{49}Fe_{51}$ alloys has a $Fm\bar{3}m$ lattice structure, in which iron and nickel atoms with a 50-50 chance are placed in surfaces or in corners of the lattice.[1,47] Here, the observed increase of lattice parameter (Table I) is possibly due to the larger atomic radius of Cr compared to that of Fe and Ni atoms in the lattice structure, since it is believed that Cr atoms are substituted for Ni or Fe atoms in γ(Fe, Ni) phase.[15]

It is reported[48] that the lattice parameter of a disordered $Ni_{50}Fe_{50}$ is larger than the $L1_0$-FeNi ordered alloys which have a $P4/mmm$ lattice structure. Therefore, the order–disorder phase transformation during the final annealing process could be also effective in variations of the lattice parameter. According to the phase diagram of Ni-Fe system, ordering transformation of $L1_0$-FeNi can occur during very slow cooling (approximately 1 °C per 4.6 billion years) at a temperature range from 350 °C to room temperature during the annealing process.[49] Also, it is shown that the addition of Cr to Ni-Fe alloys has a delaying effect on the kinetics of long-range ordering.[50] Here, this delaying effect may have led to the reduction of the degree of ordering and consequently increasing the lattice parameter for Cr-added samples (Table I). The $L1_0$-FeNi
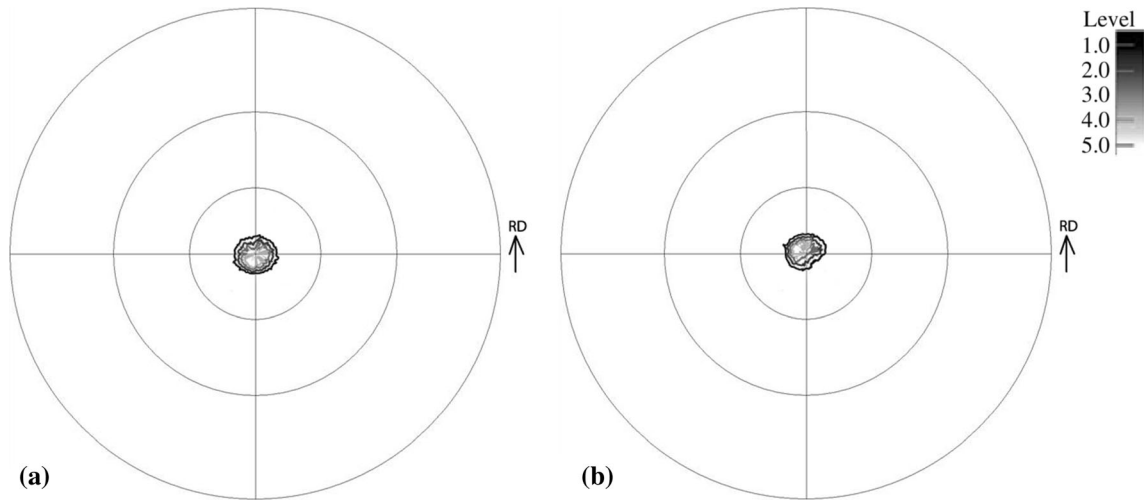

Fig. 3—(200) pole figure of the (a) 0 Cr and (b) 3 Cr samples annealed at 1150 °C.

Table I. Average Grains Size, Lattice Parameter, Resistivity, Average Vickers Microhardness for $(Ni_{49}Fe_{51})_{100-x}Cr_x$ Thin Sheets

Sample	Thickness (mm)	Grain Size (μm)	Lattice Parameter (Å)	Resistivity ($\mu\Omega$ cm)	μHardness As-Roll	Annealed (Hv)
0 Cr	0.122 ± 0.01	29 ± 15	3.5707 ± 0.002	34 ± 1.5	287 ± 8	142 ± 1
3 Cr	0.126 ± 0.01	25 ± 16	3.5786 ± 0.002	52 ± 1.5	293 ± 23	139 ± 6
7 Cr	0.114 ± 0.01	27 ± 16	3.5832 ± 0.002	79 ± 1.5	316 ± 13	137 ± 7

ordered phase is not a soft magnetic phase (since it has a coercivity of 500 to 4000 Oe).[51,52]

B. *Magnetic Properties*

Figures 4(a) through (c) show the as-captured and processed MFM images of the 0 Cr-, 3 Cr-, and 7 Cr-annealed samples. As can be seen from these figures, a labyrinthine domains structure is evident for all of the samples and the domain structure of 0 Cr sample is significantly finer than the domain structure of the Cr-added alloys. The distribution of the magnetic domain width of the samples is shown in Figure 5. It is interesting to note that the average width of magnetic labyrinthine domains is increased by increasing of Cr, *i.e.*, 1.066 , 1.319 and 1.398 μm for 0 Cr, 3 Cr, and 7 Cr samples, respectively (with a standard deviation of 0.3 μm).

Figure 6(a) displays the variation of magnetization *vs* applied field at a frequency of 50 Hz for 0 Cr-, 3 Cr-, and 7 Cr-annealed samples. As shown in Figure 6(b), the magnitude of measured saturation induction of 0 Cr sample is higher than Cr-added samples. This is mainly related to the substitution of Cr atoms as an antiferromagnetic element for Fe and Ni in the lattice structure. It is already reported that the magnetic moments of Fe and Ni atoms is reduced by substituting Cr for Fe and Ni atoms.[53] Replacing Fe and Ni with Cr atoms in the Ni-Fe phase changes the local environment of some of the Ni-Fe atoms and can give rise to the exchange weakening of two neighboring ferromagnetic atoms. Therefore, in the 0 Cr sample, a higher value of B_s (1.44 T) is obtained due to the higher concentration of Fe and Ni atoms.

Further, the squareness of the hysteresis loops, B_r/B_s, *vs* Cr content is shown in Figure 6(b). As can be seen, squareness is significantly increased for Cr-added samples compared to 0 Cr alloy. The higher level of squareness for Cr-added sample is due to the formation of a sharper cube texture, as confirmed by the pole figure results (Figure 3). Moreover, higher permeability and lower core loss at a frequency of 50 Hz obtained for the 3 Cr and 7 Cr alloys, imply significant improvement of dynamic soft magnetic properties of the Cr-added samples (Figure 6(c)).

The total core loss of annealed specimens against frequency at magnetic fields of 0.2 and 0.8 T are presented in Figures 7(a) and (b), respectively. Three
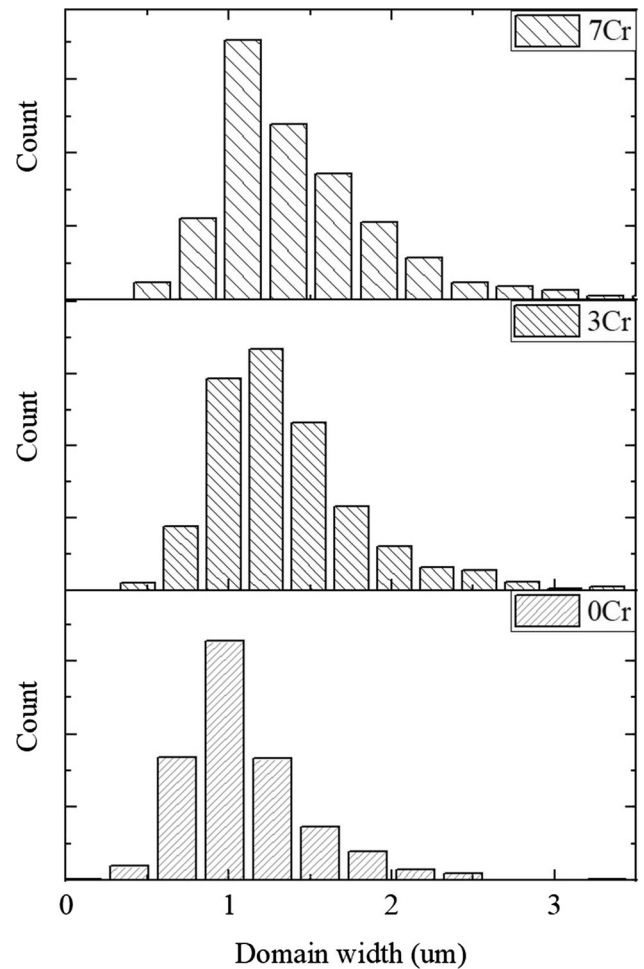

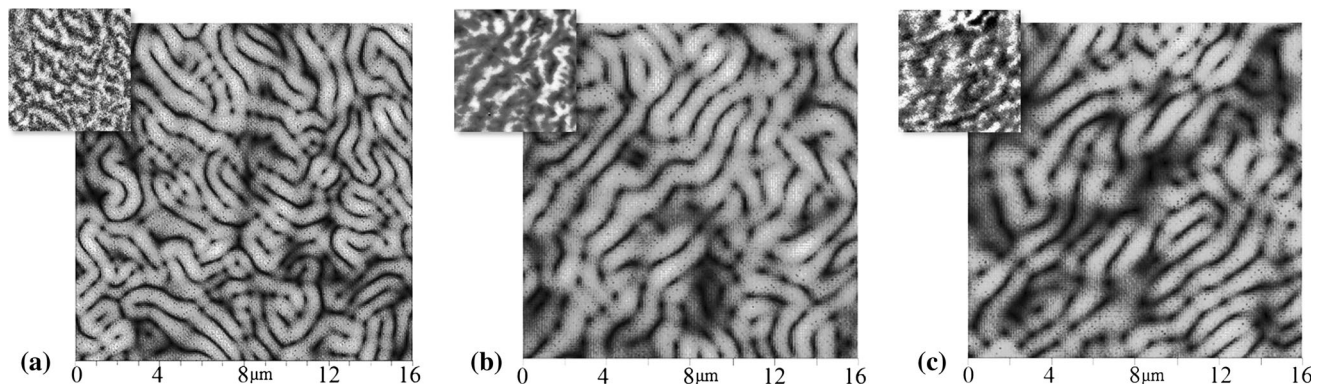Fig. 5—Distribution of domain width in the magnetic structure of the annealed samples.

Fig. 4—Raw MFM images showing magnetic stray fields scanned on the surface of the annealed samples and their processed images representing magnetic domain structure: (*a*) 0 Cr, (*b*) 3 Cr, and (*c*) 7 Cr.
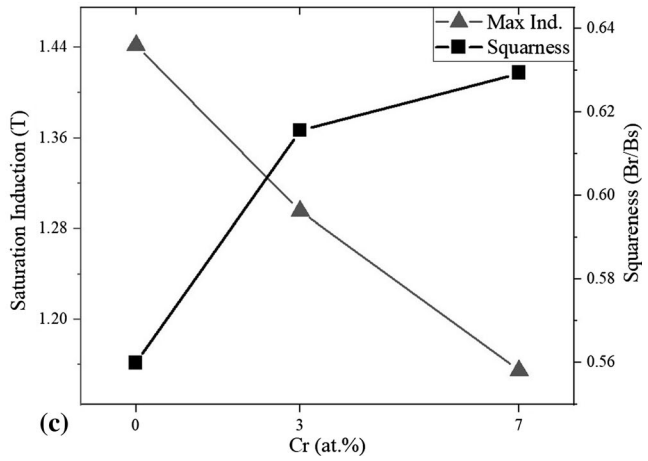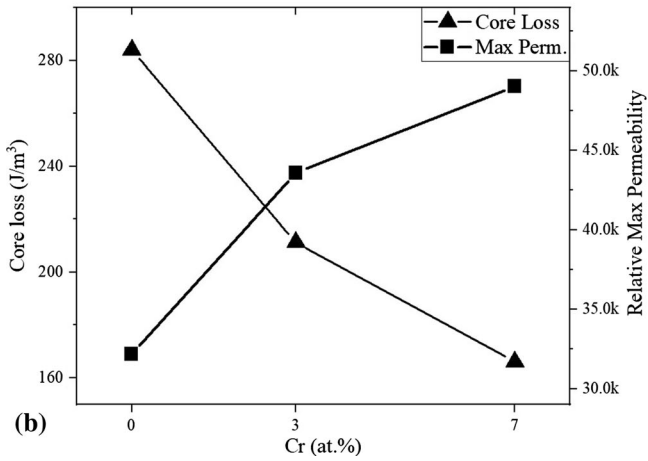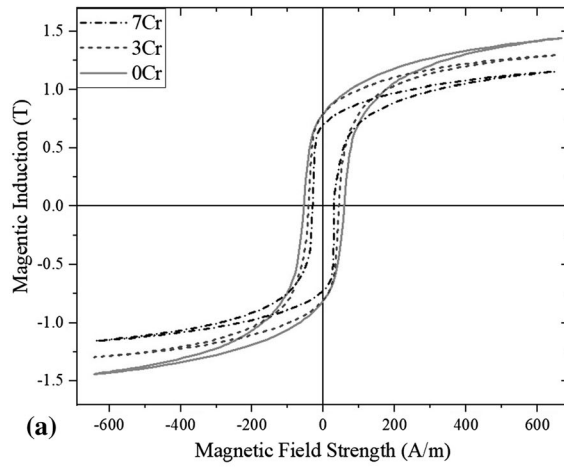
Fig. 6—(a) B-H hysteresis loops measured at $H_{max} = 650 A/m$ at $f = 50 Hz$, (b) and (c) the resultant characteristics from the loops *vs* Cr content in $(Ni_{49}Fe_{51})_{100-x}Cr_x$ system ($x = 0, 3, 7$).
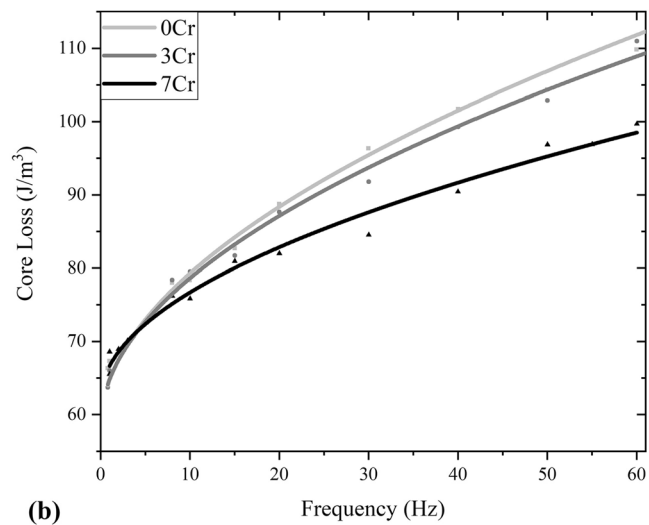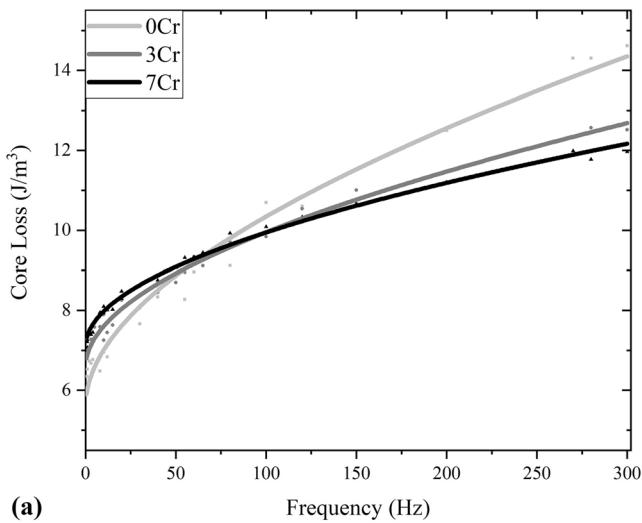

Fig. 7—Frequency dependence of the total magnetic core loss of the annealed samples, measured at (a) $B_{max} = 0.2$ T and (b) $B_{max} = 0.8 T$ where the experimental data were fitted using Eq. [5].

coefficients of the core loss in the Eq. [1] can be expressed by

$$W = C_{hys} + C_{cl}f + C_{exc}f^{1/2}, \qquad [5]$$

where $C_{hys} = 4k_{hyst}B_{max}^{\alpha}$, $C_{cl} = \pi^2 t^2 / 6\rho^{B_{max}^2}$, and $C_{exc} = k_{exc} / \sqrt{\rho}^{B_{max}^{3/2}}$ are the fitting coefficients for hysteresis loss, classic loss, and excess loss, respectively. In this equation, C_{cl} is determined by the electrical resistivity and thickness of the samples that are presented at Table I and C_{exc} and C_{hys} are determined by curve fitting of Eq. [6]. K_{hys} and α are determined by solving the first term of Eq. [5] at two different inductions, i.e., 0.2 and 0.8 T. The calculated constants of the total core loss of the samples are shown in Table II. The root of the mean square deviations between fitted and experimental values was about 1-1.5 pct, which shows a good degree of confidence between them.

The calculated classical coefficients for the annealed samples, C_{cl}, are presented in Table II, which indicates that the classical eddy current loss is decreased by the addition of 3 and 7 at. pct Cr to the $Ni_{49}Fe_{51}$ alloy. This is mainly related to the increase of resistivity in the Cr-added specimens (Table I). The measured room temperature electrical resistivity, obtained for 0 Cr, 3 Cr, and 7 Cr samples were 34, 52, and 79 $\mu\Omega$ cm, respectively. Static hysteresis coefficient (C_{hys} in Table II) was lower for 0 Cr alloy compared to those of Cr-added samples. Considering that the hysteresis loss is generally similar to the coercive force,[2,54,55] then the W_{hys} can be expressed by

$$W_{hys} \propto \frac{\sqrt{K_1/a}}{B_m d_k}. \qquad [6]$$

Therefore, the observed lower value of hysteresis loss for 0 Cr-annealed sample can be attributed as partly due to the higher value of saturation induction, B_s (Figure 7(b)) and partly due to larger grain size, d_k, for this sample compared to 3 Cr and 7 Cr samples (grain size, Table I).

As can be seen from Table II, the excess coefficient (C_{exc}) is decreased with increasing of Cr in the alloy. However, it is also observed that the addition of Cr has led to an increase in W_{exc}/W_{cls} ratio of thin sheets

Table II. Parameters of Magnetic Core Loss Obtained for the Samples

Parameter/Sample	0 Cr	3 Cr	7 Cr
C_{cl} at 0.2T (J m^{-3} s)	0.0032	0.0021	0.0011
C_{cl} at 0.8T	0.0504	0.0327	0.0173
C_{hys} at 0.2T (J m^{-3})	5.588	6.576	7.097
C_{hys} at 0.8T	58.06	58.51	62.03
C_{exc} at 0.2T (J m^{-3} s0.5)	0.4341	0.3172	0.2741
C_{exc} at 0.8T	6.548	6.249	4.575
K_{hys}	84.63	83.166	87.93
α	1.689	1.577	1.564
K_{exc}	0.00271	0.00628	0.00273
W_{exc}/W_{cl} at 0.2 T and 50 Hz	20.64	22.88	36.89

(Table II). Later case is related to coarsening effect of Cr on the domain structure of the samples (Figure 5), while the first case is due to increasing of resistivity of alloys (Table I) which is in close agreement with previous studies.[24,25,27] It is well known that the excess loss is mainly related to the micro eddy currents around the moving domain walls during magnetization process[2,11,56]; i.e., this component mainly depends on resistivity and domain structure. Further, the comparison of C_{cl} and C_{exc} data obtained for the alloys (Table II) also revealed the positive effect of Cr on the reduction of eddy current losses is more significant than the negative effect of this element on the microstructure of magnetic domains.

It is interesting to note that the total core loss for Cr-added samples was lower at 0.8 T than 0.2 T. As can be realized from Figure 7(a), the magnitude of core loss for the 7 Cr alloy is 6 pct more than that of 0 Cr sample at a frequency of 50 Hz and magnetic induction of 0.2 T (Figure 7(a)), while it is 11 pct lower at 0.8 T (Figure 7(b)). Furthermore, the core loss was 41 pct lower for 7 Cr compared to that of 0 Cr alloy at maximum induction condition (Figure 6(c)). However, the role of the efficient number of active domain walls is much more pronounced at higher B_m.[20] Therefore, the impact of the excess loss on the total loss becomes less apparent while the contribution of the eddy current loss in the total loss becomes more dominant.

IV. CONCLUSION

Based on the results obtained, it was shown that Cr has a marked effect on the magnetic domain structure and also AC magnetic properties and specially core loss of the FeNi alloy. The Cr-added thin sheets exhibited a higher power efficiency for AC applications.

(1) The formation of cube texture was confirmed for the samples cold rolled with 99 pct area reduction and annealed at 1150 °C based on our XRD and pole figure results.
(2) The addition of Cr up to 7 at. pct was found to increase the mean microhardness from 287 to 312 Hv for the as-rolled samples and to decrease from 142 to 137 Hv for the annealed samples, suggesting that the addition of Cr in $Ni_{49}Fe_{51}$ alloy accelerated the recovery and primary recrystallization during the annealing process while, postponing the secondary recrystallization.
(3) The formation of a labyrinthine stripe domain structure in all of the thin sheets was detected based on magnetic force microscopy (MFM) analysis. It was shown that by adding 7 at. pct, the domain size width is increased from 1.006 to 1.398 μm.
(4) Ultrasoft magnetic behavior was observed for the Cr-added annealed samples based on BH-hysteresis results at a frequency of 50 Hz. Permeability and squareness of Cr-added samples were increased, while maximum induction and core

loss of them were decreased compared to that of 0 Cr thin sheet.

(5) It was observed that the 0 Cr thin sheet sample has the lower loss at lower frequencies due to smaller static hysteresis loss (W_{hys}) which is believed to be related to the coarser grain size and higher saturation induction. On the other hand, it was shown that addition of Cr leads to a decrease in the contribution of the classical and excess eddy current losses (W_{cl} and W_{exc}, respectively) at higher frequencies, which consequently led to a lower total core loss. The coarser magnetic domain structure observed in the Cr-added alloys causes an increase in W_{exc}/W_{Cl} ratio, however, this negative impact on the losses was less important than the significant increase of electrical resistivity of Cr-added thin sheets.

ACKNOWLEDGMENTS

REFERENCES

1. J.R. Davis: *ASM Specialty Handbook: Nickel, Cobalt, and Their Alloys*, ASM, Cleveland, 2000.
2. H. Kronmuller and S. Parkin: *Handbook of Magnetism and Advanced Magnetic Materials*, Wiley, New York, 2007.
3. P. Ripka: *J. Magn. Magn. Mater.*, 2008, vol. 320, pp. 2466–73.
4. M.F. Littrnann, E.S. Harris: Washington, DC: U.S. Patent and Trademark Office, 1966.
5. T. Itoh, T. Omori: Washington, DC: U.S. Patent and Trademark Office, 2007.
6. L. Coutu, L. Chaput, and T. Waeckerle: *J. Magn. Magn. Mater.*, 2000, vol. 215, pp. 37–239.
7. H. Eriksson and A. Salwen: *IEEE Trans. Magn.*, 1977, vol. 13, pp. 1451–53.
8. V. Tsakiris and M. Petrescu: *Sci Bull University Politehnica of Bucharest*, 2007, vol. 69, pp. 67–78.
9. K. Gupta, K. Raina, and S. Sinha: *J. Alloy. Compd.*, 2007, vol. 429, pp. 357–64.
10. R. Casani, W. Klawitter, A. Lykens, and F. Ackermann: *J. Appl. Phys.*, 1966, vol. 37, pp. 1202–04.
11. C.W. Chen: *Magnetism and Metallurgy of Soft Magnetic Materials*, Courier Corporation, Boston, 1977.
12. R.E. Schramm and R.P. Reed: *Metallurgical and Materials Transactions A*, 1976, vol. 7, pp. 359–63.
13. L. Coutu, P.L. Reydet: Washington, DC: U.S. Patent and Trademark Office, 1998.
14. J. Mishra, S. Sahni, R. Sabat, V.D. Hiwarkar, and S.K. Sahoo: *Mater Res*, 2016, vol. 20, pp. 218–24.
15. D. Rice, J. Suits, and S. Lewis: *J. Appl. Phys.*, 1976, vol. 47, pp. 1158–63.
16. W.R. Wieserman, G.E. Schwarze, J. Niedra: 26th Intersociety Energy Conversion Engineering Conference, 1991.
17. D. Olekšáková, J. Füzer, P. Kollár, and S. Roth: *J. Magn. Magn. Mater.*, 2013, vol. 333, pp. 18–21.
18. Z. Li, K. Yao, D. Li, X. Ni, and Z. Lu: *Prog. Nat. Sci.: Mater. Int.*, 2017, vol. 27, pp. 588–92.
19. G. Bertotti and I.D. Mayergoyz: *The Science of Hysteresis: Hysteresis in Materials*, Gulf Professional Publishing, Houston, 2006.
20. G. Bertotti, F. Fiorillo, and G. Soardo: *Le Journal de Physique Colloques*, 1988, vol. 49, pp. 1915–19.
21. F. Brailsford: *Physical principles of magnetism*, Van Nostrand, New York, 1966.
22. K. Overshott: *IEEE Trans. Magn.*, 1981, vol. 17, pp. 2698–2700.
23. H. Williams, W. Shockley, and C. Kittel: *Phys. Rev.*, 1950, vol. 80, pp. 1090–94.
24. R. Pry and C. Bean: *J. Appl. Phys.*, 1958, vol. 29, pp. 532–33.
25. E. Lee: *Proc. IEE-Part C: Monogr.*, 1958, vol. 105, pp. 337–42.
26. J. Bishop: *J. Magn. Magn. Mater.*, 1985, vol. 49, pp. 241–49.
27. G. Bertotti: *IEEE Trans. Magn.*, 1988, vol. 24, pp. 621–30.
28. K. Overshott and M. Price: *IEEE Trans. Magn.*, 1982, vol. 18, pp. 1394–96.
29. A. Hubert and R. Schäfer: *Magnetic Domains: The Analysis of Magnetic Microstructures*, Springer, Berlin, 2008.
30. D.C. Zipperian: *Metallographic Handbook*, PACE Technologies, Tucson, 2011.
31. B.D. Cullity: *Elements of X-ray Diffraction, Second*, Edition ed., Addison-Wesley Publishing Company Inc., Reading, 1978.
32. I. Miccoli, F. Edler, H. Pfnür, and C. Tegenkamp: *J. Phys.: Condens. Matter*, 2015, vol. 27, p. 223201.
33. A753-08 "Standard Specification for Wrought Nickel-Iron Soft Magnetic Alloys (UNS K94490, K94840, N14076, N14080)," ASTM International, West Conshohocken, PA, 2013.
34. I. Baker, H. Chang, and J. Li: *MRS Online Proceedings Library Archive*, 2004, vol. 819, p. 819.
35. R.E. Smallman and R.J. Bishop: *Modern physical metallurgy and materials engineering*, Elsevier, Amsterdam, 1999.
36. J. Bailey and P.B. Hirsch: *Proceedings Mathematical Physical & Engineering Sciences*, 1962, vol. 267, pp. 11–30.
37. F. Rhines and B. Patterson: *Metall. Trans. A*, 1982, vol. 13, pp. 985–93.
38. S. Gražulis, D. Chateigner, R.T. Downs, A. Yokochi, M. Quirós, L. Lutterotti, E. Manakova, J. Butkus, P. Moeck, and A. Le Bail: *J. Appl. Crystallogr.*, 2009, vol. 42, pp. 726–29.
39. B. Hutchinson: *Materials Science Forum Conference*, 2012, vol. 702, pp. 3–10.
40. H. Hu: *Texture Stress Microstruct.*, 1974, vol. 1, pp. 233–58.
41. E. Specht, A. Goyal, D. Lee, F. List, D. Kroeger, M. Paranthaman, R. Williams, and D. Christen: *Supercond. Sci. Technol.*, 1998, vol. 11, p. 945.
42. S. Rothman, L. Nowicki, and G. Murch: *J. Phys. F: Met. Phys.*, 1980, vol. 10, p. 383.
43. M. Čebron and F. Kosel: *Strojniški vestnik—J. Mech. Eng.*, 2014, vol. 60, pp. 462–74.
44. P.A. Beck and H. Hu: *J. Miner. Metals Mater. Soc.*, 1952, vol. 4, pp. 83–90.
45. F. Caleyo, T. Baudin, and R. Penelle: *Eur. Phys. J. Appl. Phys.*, 2002, vol. 20, pp. 77–89.
46. L. Swartzendruber, V. Itkin, and C. Alcock: *J. Phase Equilib.*, 1991, vol. 12, pp. 288–12.
47. A.D.G. Cacciamani, M. Palumbo, and A. Pasturel: *Intermetallics*, 2010, vol. 1, pp. 1148–62.
48. A. Bradley, A. Jay, and A. Taylor: *Lond. Edinb. Dublin Philos. Mag. J. Sci.*, 1937, vol. 23, pp. 545–57.
49. K. Reuter, D.B. Williams, and J. Goldstein: *Metall. Trans. A*, 1989, vol. 20, pp. 719–25.
50. A. Marucco: *Key Eng. Mater. Conf.*, 1991, vol. 48, pp. 77–90.
51. J. Albertsen, J. Knudsen, G. Jensen, and J. Danon: *Meteoritics*, 1978, vol. 13, pp. 379–83.
52. T. Nagata, J.A. Danon, and M. Funaki: *Memoirs Natl. Inst. Polar Res.*, 1987, vol. 46, pp. 263–82.
53. J.S. Wróbel, D. Nguyen-Manh, M.Y. Lavrentiev, M. Muzyk, and S.L. Dudarev: *Phys. Rev. B*, 2015, vol. 91, p. 024108.
54. E. Adler and H. Pfeiffer: *IEEE Trans. Magn.*, 1974, vol. 10, pp. 172–74.
55. F. Pfeifer and C. Radeloff: *J. Magn. Magn. Mater.*, 1980, vol. 19, pp. 190–207.
56. J. Bishop: *Br. J. Appl. Phys.*, 1966, vol. 17, p. 1451.